Electronic Supplementary Material (ESI) for Nanoscale.

Electronic Supplementary Information

Magnetron-sputtered copper nanoparticles: lost in gas aggregation and found by *in situ* X-ray scattering

Jaroslav Kousal, Artem Shelemin, Matthias Schwartzkopf, Oleksandr Polonskyi, Jan Hanuš, Pavel Solař, Mykhailo Vaidulych, Daniil Nikitin, Pavel Pleskunov, Zdeněk Krtouš, Thomas Strunskus, Franz Faupel, Stephan V. Roth, Hynek Biederman, and Andrei Choukourov

1. Experimental details

The GAS consisted of a cylindrical vacuum chamber (100 mm in diameter) with water-cooled walls. A moveable 3-inch magnetron with a copper target was installed at one side of the GAS whereas the opposite side ended with an orifice which was 4 mm long and 3 mm in diameter. The magnetron was equipped with a set of permanent magnets that provided a circular plasma ring with the radius of about 20 mm above the target. The profile of the magnetic field was measured and is shown in Figure S 1.

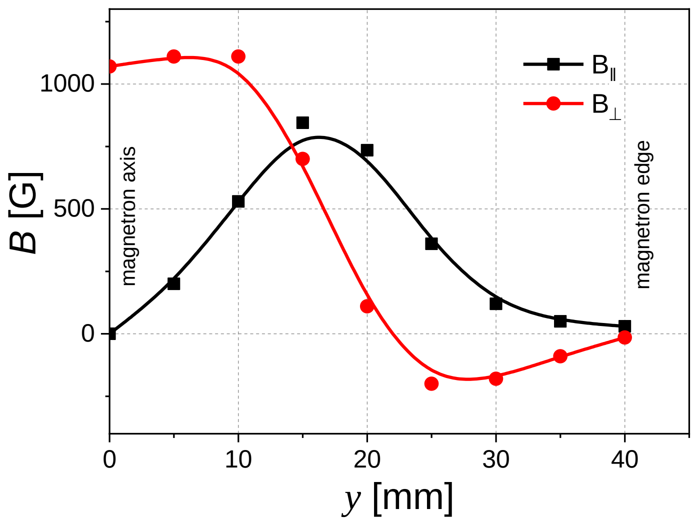

Figure S 1 Intensity of the magnetic field B measured in the parallel ($B_{\parallel}$) and the normal ($B_{\perp}$) direction to the target plane from the magnetron axis, across its radius and to the magnetron edge. The zero distance corresponds to the magnetron axis.

Two opposing windows (40 mm in diameter, made of 125-µm thick Kapton™ foils) were placed on transversal ports of the GAS. The ports were equipped with cylindrical baffles (25 mm in diameter) to minimize the deposition of NPs on the inner side of the windows. The GAS was connected *via* its orifice to another vacuum chamber through which pumping with rotary and turbomolecular pumps was performed.

The setup was installed at the P03 beamline of PETRA III, DESY, Hamburg, Germany. The synchrotron provides a brilliance exceeding 10^{21} photons/(s mm^2 mrad^2). The storage ring operates at 99.5 ± 0.5 mA beam current in a top-up mode keeping the stability of the photon flux at 1%. The X-ray was focused to an ellipsoidal beam of 22.0 × 32.0 ± 0.5 µm (V × H axes) and passed through the transversal ports of the GAS to reach a Pilatus 1M detector (Dectris Ltd., pixel size 172 µm) which was placed 5596.0 ± 0.5 mm away from the axis of the GAS chamber with an evacuated pathway in between. The GAS and the pumping system were fixed at a goniometer table (HUBER Diffraktionstechnik GmbH) that allowed horizontal and vertical positioning with respect to the X-ray beam. Together with the travel distance of the moveable magnetron, it allowed sampling the inner volume of the GAS within the range of x = 0 – 40 mm and y = ± 12 mm, where x is the axial distance from the magnetron and y is the radial distance measured from the magnetron axis. Constant Ar pressure of 86 Pa and the flow rate of 25 sccm were used. The magnetron was run by a DC generator (Advanced Energy MDX500) with the current and voltage set at 500 mA and 320 V, respectively.

2. System calibration

Two types of standards with the known d-spacing were used to calibrate the sample-to-detector distance. These included collagen (from chicken tendon) and silver behenate ($AgC_{22}H_{43}O_2$), the d-spacing of which was 65 nm and 5.837 nm, respectively. The calibration sample was placed inside the aggregation chamber at the position corresponding to the axis of the magnetron and under atmospheric pressure. The X-ray scattering patterns were acquired with the photon energy in the primary beam of 13.01 keV and the wavelength of 0.941 nm. The calibration was done using a SAXS/WAXS calibration tool in DPDAK. The beam centre was defined as x = 549.16 pixel and y = 293.49 pixel; the detector tilt and rotation were at 0°. The obtained sample-to-detector distance was 5596.0 ± 0.5 mm.

The transmission coefficient T = I_1/I_0 = 0.98 was calculated for the cases with maximal scattering intensity where I_1 is the intensity of the beam after the calibration sample insertion and I_0 is the intensity of the primary beam, both measured at the beam stop.

3. Data acquisition and processing

3.1. Time-averaged measurements

3.1.1. Data acquisition

For each of the spatial position (x, y) inside the GAS, the plasma was turned on, the discharge was allowed to stabilize for 2 s, a diffraction image was acquired with the exposure time of 15 s (Figure S 2), and the plasma was turned off. The experiment was repeated 16 times for a certain spatial position and then the position was changed. A background signal was recorded for 1 s before and after each of the plasma runs (Figure S 3). It was found to be identical (Figure S 4), thus confirming the absence of the NP deposition on the Kapton windows.

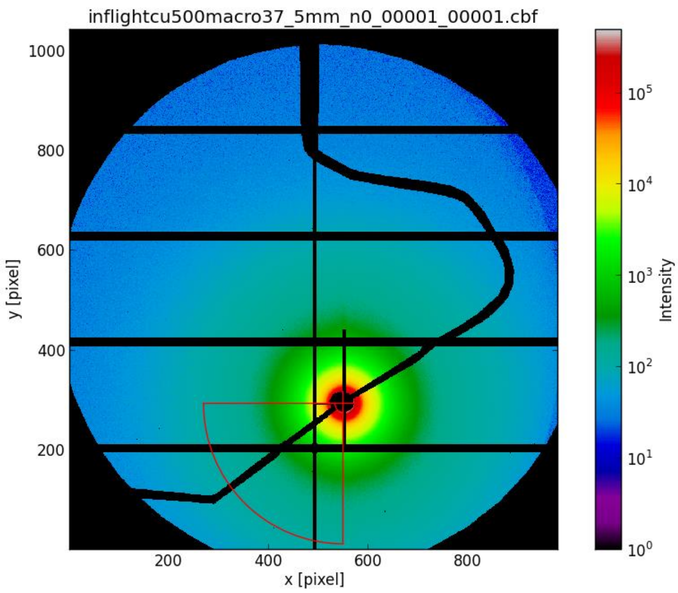

Figure S 2 Full scattering pattern on the detector with the integration sector used in DPDAK for the data processing. The mask allowing for the compensation of blank pixels, the beam stop and the residual direct beam scattering was applied.

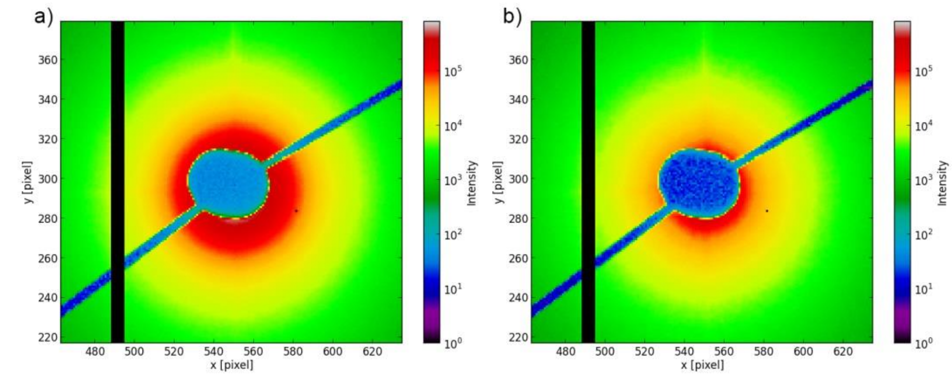

Figure S 3 Two-dimensional diffraction images from the SAXS detector sampled at the axial distance of x = 5.0 mm and at the radial distance of y = 0.0 mm: a) during the NP production when the discharge is on; b) background signal obtained when the discharge is off.

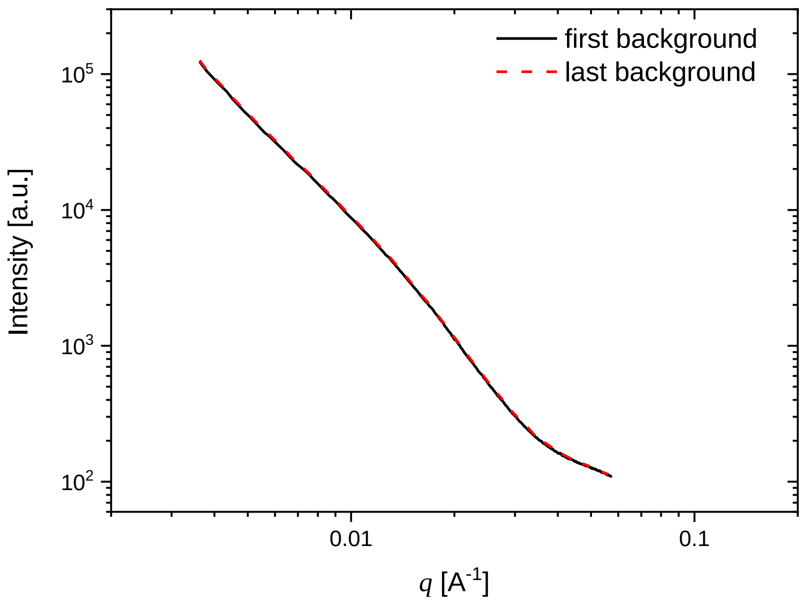

Figure S 4 The background signal (in terms of integrated scattered intensity I vs. scattering wave vector q, see below) acquired before the first and after the last (16th) SAXS measurement at the same spatial position with the axial distance of x = 5.0 mm and with the radial distance of y = 0.0 mm.

The calibration of raw data, their reduction and integration was performed using the software DPDAK, a customizable code for the analysis of large SAXS data. For each of the spatial position (x, y), each of 16 diffraction images and 16 background signals was integrated within the range of q = 0.0036 – 0.057 Å^{-1}, where $q = 4\pi \sin(\theta)/\lambda$ is the magnitude of the scattering vector, θ is the scattering angle and λ is the wavelength of the X-rays. Thus, the integrated scattered intensity I vs. scattering wave vector q curves were obtained. The examples of the curves for the data, for the background and for the difference between them are shown in Figure S5. The scattering curves with subtracted background (no correction factor applied) were averaged to obtain a single scattering curve for each of the spatial positions (x, y) as shown in Figure S5.

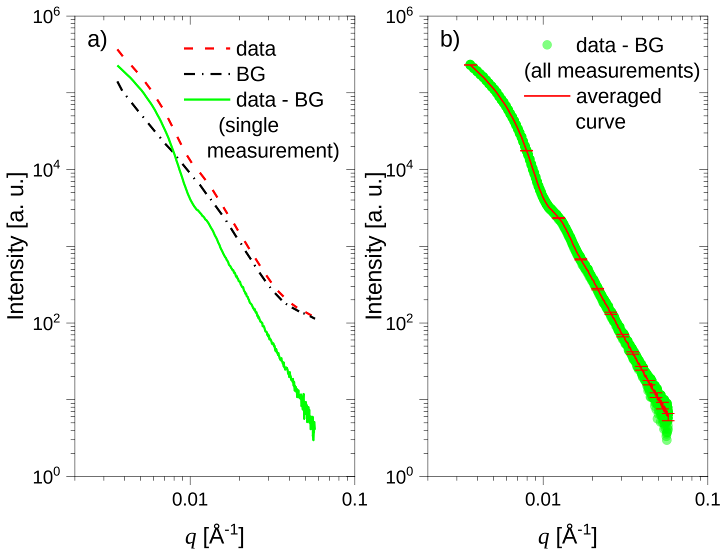

Figure S5 Integrated scattered intensity I as a function of scattering wave vector q at x = 5.0 mm and y = 0.0 mm: a) examples obtained from one data and background (BG) acquisition when the discharge is on and off, respectively, and the difference between the two; b) several data sets with subtracted BG are used to obtain the average scattering curve for this spatial position; error bars correspond to standard error of the mean.

3.1.2. Fitting of the scattering curves

The averaged scattering curves for each of the spatial positions (x, y) were fitted with a full sphere model, as implemented in the SASView software package:

$$I(q) = \frac{volume\ fraction}{V}\left[3V(\Delta\rho)\frac{\sin(qr) - qr\cos(qr)}{(qr)^3}\right]^2$$

Here, V is the volume of the scatterer particle, r is the radius of a spherical NP, $\Delta\rho$ is the difference between the scattering length densities of the scatterer and of the medium. The scattering length densities of the NPs and of the medium were set to the values corresponding to bulk copper and to argon at the working pressure inside the GAS. The error weights for fitting were taken as $\sqrt{I(q)}$. Lognormal size distribution was adopted for the calculation of the mean NP size (diameter):

$$f(x) = \frac{1}{N_{orm}}\frac{1}{x\sigma}e^{-\frac{(\ln(x) - \ln(x_{med}))^2}{2\sigma^2}}$$

$$\mu = e^{\ln(x_{med}) + \sigma^2/2}$$

Here, x_{med} and μ are the median and the mean values of the size distribution, σ is standard deviation and N_{orm} is the normalization factor.

Fitting over the entire range of q = 0.0036 – 0.057 Å^{-1} gives a better fit for the data sets obtained for zone II (Figure S 6a), where the overall scattering intensity is higher, and a worse fit for other zones (for example, zone III, Figure S6 b) with lower scattering intensity. In all the cases, the fits are not perfect, which implies that the real size distribution of the NPs may deviate from the idealistic lognormal distribution. Nonetheless, our simplified approach is sufficient to describe the growth of the NPs in the GAS. Two other fitting scenarios were also tested: 1) for q < 0.01 Å^{-1} to account for the larger NPs and 2) for q > 0.01 Å^{-1} to account for the smaller NPs. In the case of zone II, both of the additional scenarios give the results which are almost identical to the fitting over the entire range of q whereas for zone III, separate processing of the regions with low and high q helps to improve the fitting.

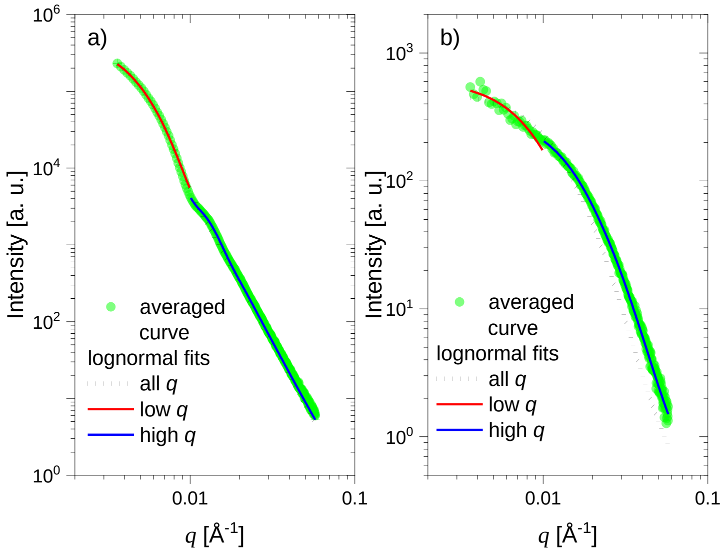

Figure S 6 Examples of the fitting of the average scattering curves for two different spatial positions in the GAS: a) x = 5.0 mm, y = 0.0 mm (zone II); b) x = 15.0 mm, y = 0.0 mm (zone III). The data points are fitted with the full sphere model of SASView using the lognormal distribution over the entire range of q as well as for the range of q < 0.01 Å^{-1} and q > 0.01 Å^{-1}.

The results of the fitting are shown in terms of the NP relative volume ratio and the NP diameter in dependence on the axial and the radial distance in Figure S 7 and Figure S 8. All the fitting scenarios are taken into account here including fitting over the entire range of q as well as separate fitting for q < 0.01 Å^{-1} and q > 0.01 Å^{-1}. Regardless of the fitting method used, the trends in the evolution of the NP relative volume fraction and the NP diameter remain conserved and as described in the main text (where only the results from the fitting over the entire range of q are shown for simplicity). The absolute values of these parameters do show a certain deviation which also points to the possibility that the real size distribution of the NPs in the GAS may be more complex.

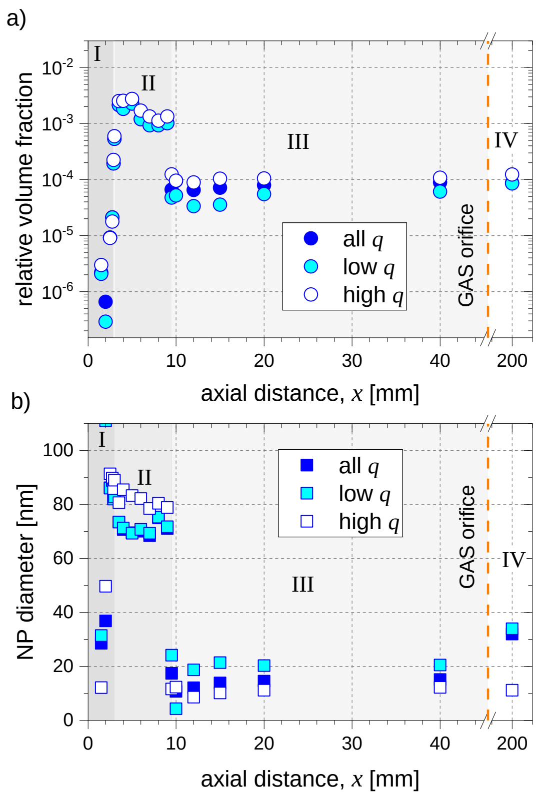

Figure S 7 Results of fitting of average scattering curves for the entire range of q, for $q < 0.01$ Å^{-1} (low q) and for $q > 0.01$ Å^{-1} (high q): a) relative volume fraction; b) mean diameter of the Cu NPs in dependence on the axial distance in the GAS and with the radial distance fixed at $y = 0.0$ mm. Roman numerals correspond to different NP growth zones as described in the main text.

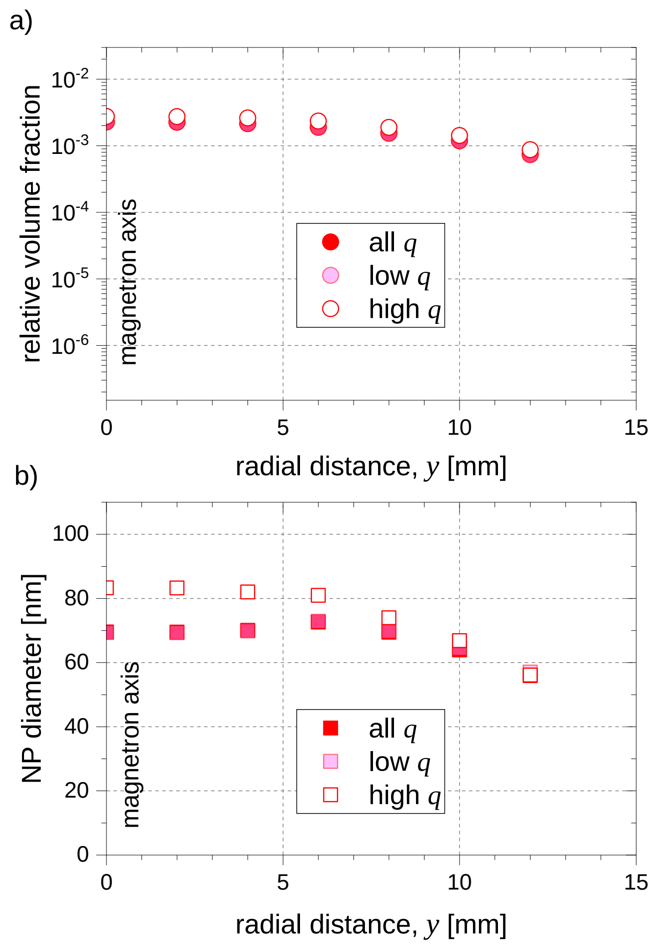

Figure S 8 Results of fitting of average scattering curves for the entire range of q, for $q < 0.01$ Å^{-1} (low q) and for $q > 0.01$ Å^{-1} (high q): a) relative volume fraction; b) mean diameter of the Cu NPs in dependence on the radial distance in the GAS and with the axial distance fixed at $x = 5.0$ mm.

The assumption of the complex size distribution finds further validation by performing the fitting of the average scattering curves in the IgorPro/Irena software package. Figure S 9 shows the examples of the relative volume distribution of the NP size generated in IgorPro/Irena by the method of Maximal Entropy for the axial positions of $x = 5.0$ mm (zone II) and $x = 15.0$ mm (zone III). Zone III is dominated by small NPs in agreement with the results of the SASView fitting (Figure S 7). Zone II is characterized by the shift of the distribution maximum to a larger size. Nevertheless, a substantial contribution from small particles is still present here as manifested in the change of the skewness of the distribution. We attribute this effect to the transverse inhomogeneity of the NP size distribution in the volume sampled by X-ray. Here, the X-ray beam propagates through the plasma ring, then it crosses the central trapping region and exits again through the plasma ring (see Scheme 1 in the main text). Thus, the scattering curves in this region are a superposition of the signals from smaller NPs present in the vicinity of the plasma ring and bigger NPs captured close to the magnetron axis (see also Scheme 2 of the main text).

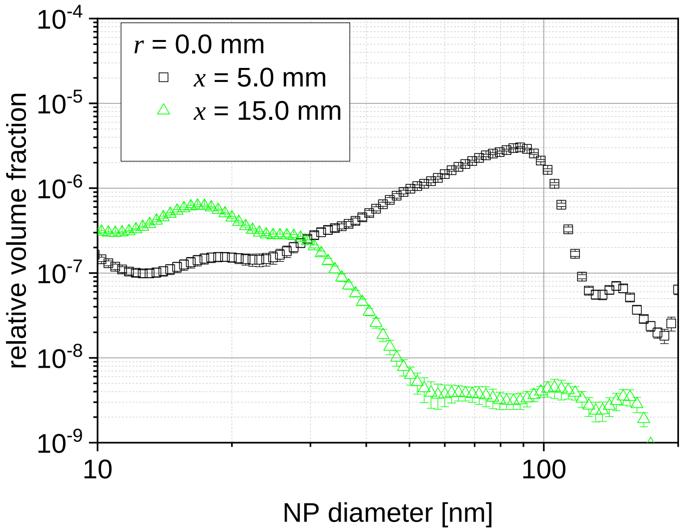

Figure S 9 Volume distribution of the NP size calculated in IgorPro/Irena for two axial positions of x = 5.0 mm (zone II) and x = 15.0 mm (zone III).

3.2. Time-resolved measurements

Time-resolved measurements were performed, with the detector scanning routine being synchronized with the DC source. The discharge was repeatedly run for 9 s followed by the 6 s off-time, giving the pulse period of 15 s. The diffraction images were acquired along the axis of the aggregation chamber (y = 0.0 mm) at different positions from the magnetron target. The diffraction images were obtained with a frequency of 10 images per second, with 50 ms acquisition time per image and 50 ms read-out time. The background signal was recorded for 1 s before and after each of the plasma runs. Both the diffraction and the background signals were integrated and the background was subtracted as described above. An example of the time series of the curves $I(q,t,x$ = 5.0 mm, y = 0.0 mm) is shown in Figure S 10.

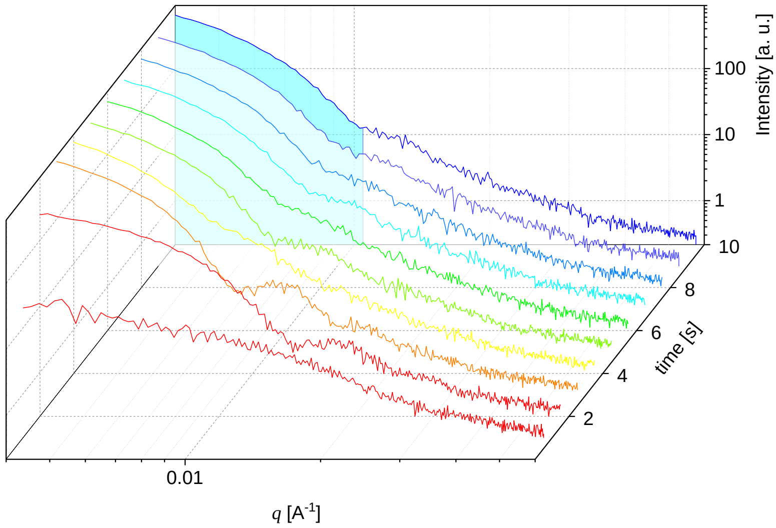

Figure S 10 Scattered intensity as a function of q and time at the axial position of x = 5.0 mm and the radial position of y = 0.0 mm. The shaded area designates the integral $\int_{0.0036\ \text{Å}^{-1}}^{0.0119\ \text{Å}^{-1}} I(q)\, dq$, the values of which were used to build the time-resolved contour plot in Figure 5 of the main text.

For all the $I(q)$ curves, the low-q region was chosen from the beam stop to the roundabout of the first minimum and the value $\int_{0.0036\ \text{Å}^{-1}}^{0.0119\ \text{Å}^{-1}} I(q)\, dq$ was calculated (see also the diffraction pattern shown in Figure S 11). The contour plot of this value in dependence on time and axial position was constructed and shown in the main text as Figure 5.

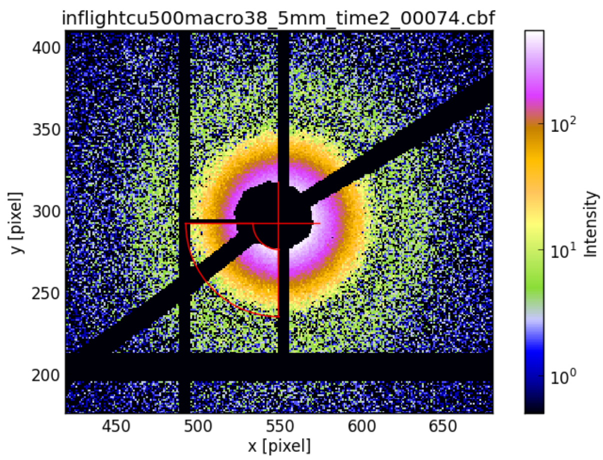

Figure S 11 Detail of a scattering pattern on the detector from the time-resolved measurements with the sector used for obtaining the integrated intensity shown by red lines. The mask was applied.

The velocity of the NP propagation after switching off the discharge was compared with the linear velocity of the Ar flow. The latter was calculated as:

$$v = P_0 Q_0 / PA$$

Here, P_0 is standard pressure, Q_0 is the Ar flow at standard pressure, P is the pressure inside the GAS, A is the cross-sectional area of the GAS. For Q_0 = 25 sccm = 4.2×10^{-7} m^3/s, P = 86 Pa and A = 0.00785 m^2 used in this work the linear gas velocity is v = 0.06 m/s.